Wen et al. *Light: Science & Applications* (2024)13:88
https://doi.org/10.1038/s41377-024-01396-3

Official journal of the CIOMP 2047-7538
www.nature.com/lsa

ARTICLE Open Access

Metasurface array for single-shot spectroscopic ellipsometry

Shun Wen[1], Xinyuan Xue[1], Shuai Wang[1], Yibo Ni[1], Liqun Sun[1] and Yuanmu Yang[1]✉

Abstract

Spectroscopic ellipsometry is a potent method that is widely adopted for the measurement of thin film thickness and refractive index. Most conventional ellipsometers utilize mechanically rotating polarizers and grating-based spectrometers for spectropolarimetric detection. Here, we demonstrated a compact metasurface array-based spectroscopic ellipsometry system that allows single-shot spectropolarimetric detection and accurate determination of thin film properties without any mechanical movement. The silicon-based metasurface array with a highly anisotropic and diverse spectral response is combined with iterative optimization to reconstruct the full Stokes polarization spectrum of the light reflected by the thin film with high fidelity. Subsequently, the film thickness and refractive index can be determined by fitting the measurement results to a proper material model with high accuracy. Our approach opens up a new pathway towards a compact and robust spectroscopic ellipsometry system for the high throughput measurement of thin film properties.

Introduction

For semiconductor processing, such as in the manufacturing of integrated circuits and flat display panels, to ensure processing quality and efficiency, it is crucial to accurately measure the thickness and optical constant of nanometer-scale thin films in a high throughput[1–4]. Instruments such as white-light interferometers, scanning electron microscopes, and atomic force microscopes may allow the measurement of film thickness with high accuracy, yet they have a relatively slow measurement speed and high system complexity. The measurement may also require direct contact with the sample under test. Spectroscopic ellipsometry is an alternative method that enables highly accurate and non-destructive measurements of thin film thickness as well as its optical constant, which has been widely implemented in semiconductor metrology and process monitoring[5–7].

In a typical spectroscopic ellipsometry system, it first measures the change in the polarization state of light reflected from the thin film under test. The wavelength-dependent complex reflectance ratio ρ between p- and s-polarized light, or the ellipsometry parameters of the thin film is written as,

$$\rho = \tan(\Psi)e^{i\Delta} \tag{1}$$

where $\tan(\Psi)$ and Δ represent the amplitude ratio and phase difference, respectively. After experimentally obtaining the ellipsometry parameters, it is fitted to a theoretical model to eventually determine the thin film thickness and optical constant.

A conventional spectroscopic ellipsometer typically modulates the polarization state via mechanical rotation of the compensator or analyzer[8–10], which may result in a large size and its sensitivity to mechanical vibration noise. To realize polarization modulation without moving parts, one may resort to photoelastic or electro-optic effects[11]. Single-shot Stokes ellipsometry[12] has also been demonstrated based on the division-of-amplitude method using multiple beam splitters and polarizing prisms. For the

Correspondence: Yuanmu Yang (ymyang@tsinghua.edu.cn)
[1]Department of Precision Instrument, State Key Laboratory of Precision Measurement Technology and Instruments, Tsinghua University, Beijing 100084, China
These authors contributed equally: Shun Wen, Xinyuan Xue

© The Author(s) 2024
Open Access This article is licensed under a Creative Commons Attribution 4.0 International License, which permits use, sharing, adaptation, distribution and reproduction in any medium or format, as long as you give appropriate credit to the original author(s) and the source, provide a link to the Creative Commons licence, and indicate if changes were made. The images or other third party material in this article are included in the article's Creative Commons licence, unless indicated otherwise in a credit line to the material. If material is not included in the article's Creative Commons licence and your intended use is not permitted by statutory regulation or exceeds the permitted use, you will need to obtain permission directly from the copyright holder. To view a copy of this licence, visit http://creativecommons.org/licenses/by/4.0/.

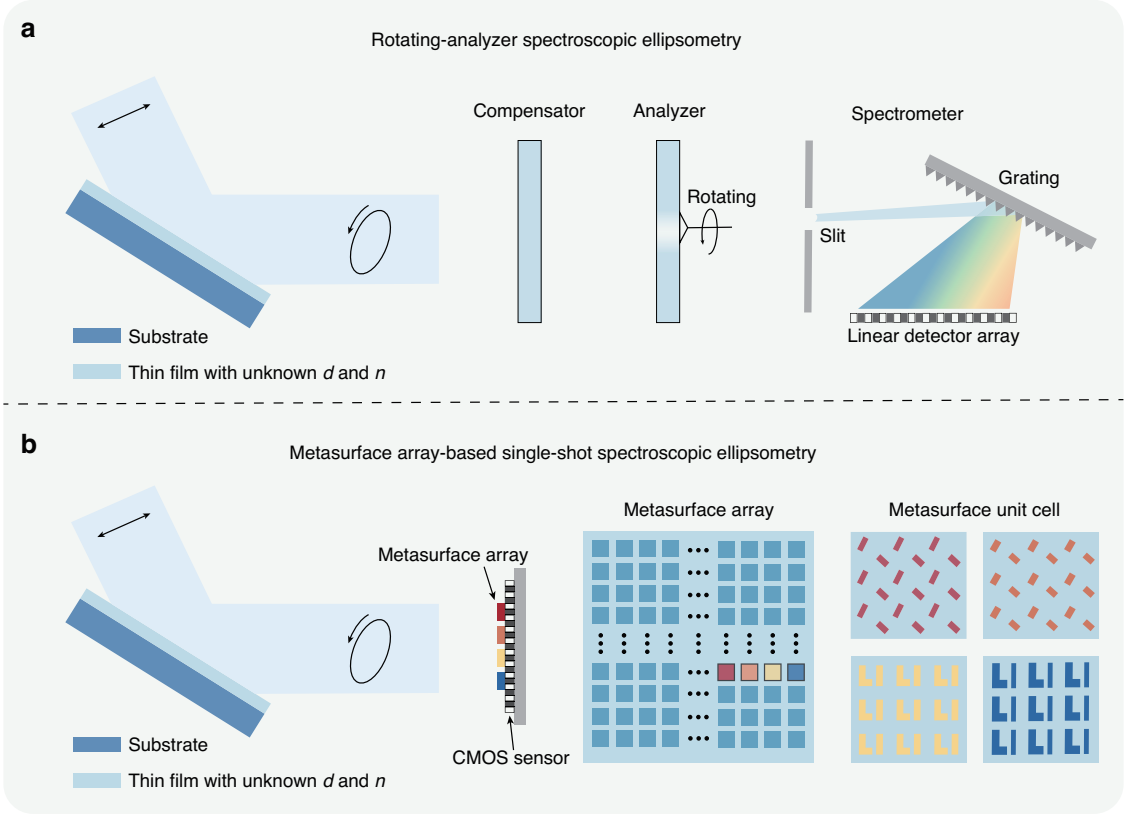

Fig. 1 Comparison between conventional and metasurface array-based spectroscopic ellipsometry. a Schematics of a conventional spectroscopic ellipsometry system equipped with a compensator, a mechanically-rotating analyzer, and a grating-based multi-channel spectrometer. The thickness *d* and refractive index *n* of the thin film can be determined by fitting the measured ellipsometry parameters with a theoretical model. **b** Schematics of a metasurface array-based single-shot spectroscopic ellipsometry system. The metasurface array, with each unit cell designed to support anisotropic and spectrally-diverse response, is used to encode the full Stokes polarization spectrum of light reflected from the thin film onto a CMOS image sensor. The ellipsometry parameters can be computationally reconstructed and used to determine the thin film properties. CMOS complementary metal-oxide semiconductor

spectral detection, an ellipsometer often uses a grating-based spectrometer[13,14]. The combination of fast polarization modulation and multichannel spectral detection have enabled real time ellipsometry measurements[3,15,16] towards various applications[17]. Nonetheless, a typical spectroscopic ellipsometer, as shown in Fig. 1a, requires a cascade of polarization-modulation and spectral detection system. Recently, alternative methods, such as dual-comb spectroscopic ellipsometry[18,19], have been proposed to partially address the abovementioned issues. However, dual-comb spectroscopic ellipsometry may have a limited spectral range for measurement, requires high-cost light sources, and also does not permit single-shot measurements.

Metasurface[20–24] is an emerging class of planar optical elements that allows extremely versatile manipulation of the amplitude[25,26], phase[27,28], polarization[29–31], and spectrum[32,33] of light at the subwavelength scale. Therefore, it may offer a new route toward constructing compact single-shot spectropolarimetric measurement systems. Recently, polarization-sensitive metalens arrays[34–37] and metasurface-based polarization gratings[38–40] have been utilized to build single-shot full Stokes polarization detection and imaging systems. On the other hand, to realize a compact spectrometer, one may design a metasurface-based narrowband filter array[41,42], with each filter responsible for transmitting a specific wavelength. Yet, a narrowband filter array intrinsically has a low light throughput. More recently, there has been a growing interest to develop metasurface-based miniaturized spectrometers[43–47] and hyperspectral imaging systems[48–51] based on computational reconstruction. In this approach, a metasurface filter array with a random spectral response is coupled with an iterative optimization algorithm or deep learning to reconstruct the spectrum, thus offering a higher light throughput and less stringent metasurface design requirement. For metasurface-based computational spectrometers, one of the prerequisites of the robust reconstruction of the spectral information is the construction of a filter array with a low spectral correlation and the accurate calibration of the filter response. However, due to

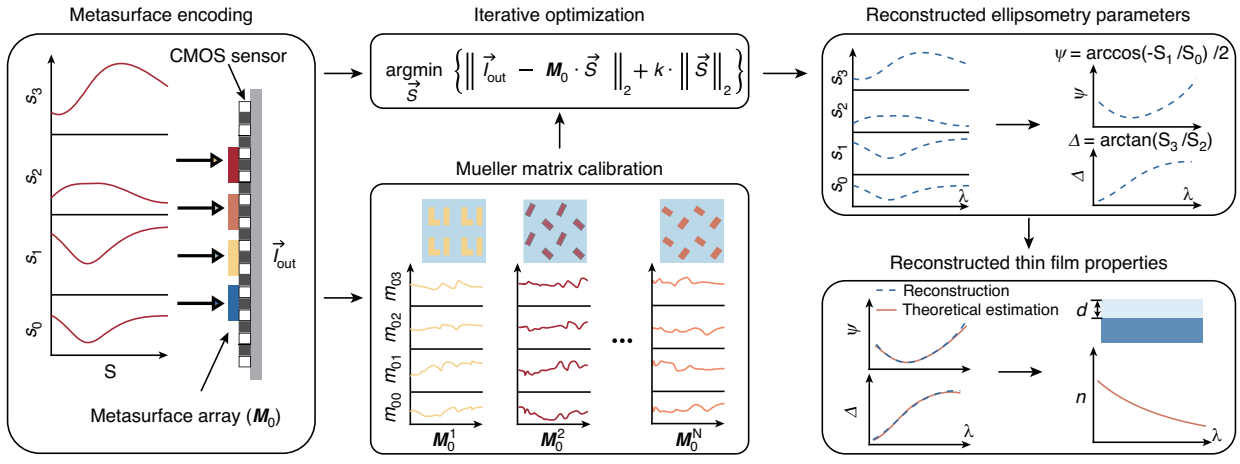

Fig. 2 Working principle of the metasurface array-based single-shot spectroscopic ellipsometry. The prototype consists of a single-layer metasurface array integrated on top of a CMOS image sensor. The Mueller matrix of the metasurface array ($\boldsymbol{M}_0$) is pre-calibrated. Together with the measured intensity on the imaging sensor (I_{out}), the full Stokes polarization spectrum of the incident light can be reconstructed by a convex optimizer with l_2-regularization. In the following, the reconstructed full Stokes polarization spectrum can be converted to the ellipsometry parameters for the determination of thin film thickness d and refractive index n by fitting the measurement with a multi-beam interference model

the angle- and polarization-dependent response of most metasurface-based filters, accurate spectral reconstruction may become rather challenging for generic applications that involve light with a wide range of incident angles and polarization states.

Some recent studies have also aimed at using metasurface for simultaneous spectropolarimetric detection[52–57]. For instance, a metasurface-based polarization grating has been utilized for splitting light with different spectral and polarization components in the spatial domain[52,53]. However, similar to a conventional grating-based spectrometer, spectropolarimetry based on polarization grating has a fundamental tradeoff between the optical path length (system form factor) and the spectral resolution. We recently demonstrated computational spectropolarimetry based on a tunable liquid crystal-integrated metasurface[57], yet it requires active tuning elements and does not allow single-shot measurement. In addition, its spectral measurement range is limited to the near-infrared range.

In this work, we propose and experimentally demonstrate a single-shot spectroscopic ellipsometry system using a passive silicon-based metasurface array for spectropolarimetric encoding in the visible frequency regime, with the system schematically depicted in Fig. 1b. The metasurface unit cell is meticulously designed to exhibit rich and anisotropic spectral features. Combining a single-shot measurement taken by the CMOS sensor with a straightforward iterative optimization algorithm, the full Stokes polarization spectrum of light reflected by the thin film can be reconstructed in high fidelity. Subsequently, the thickness and refractive index of the thin film can be obtained by fitting the measured ellipsometry parameters with a theoretical model. For the proposed ellipsometry system, light impinges on the metasurface filter array at a near-normal incident angle, resulting in a well-calibrated filter response, thus allowing the robust reconstruction of the spectropolarimetric information.

Results

The detailed working principle of the metasurface array-based spectroscopic ellipsometry is schematically illustrated in Fig. 2. The full Stokes polarization spectrum of light impinging on the metasurface array can be expressed as $\vec{S}(\lambda) = [s_0(\lambda), s_1(\lambda), s_2(\lambda), s_3(\lambda)]^{\mathrm{T}}$. The metasurface array consists of N elements and its polarization-dependent transmittance spectrum can be described by a Mueller matrix $\boldsymbol{M}(\lambda)$, which is a function of the wavelength λ. The transmitted light with its intensity recorded by the CMOS sensor corresponds to the first element s_0 in a Stokes vector, which can be expressed as,

$$\vec{I}_{\mathrm{out}} = \sum_{\mathrm{i}=1}^{l} \mathbf{M}_0(\lambda_i) \cdot \vec{S}(\lambda_i) = \mathbf{M}_0 \cdot \vec{S} \tag{2}$$

where $\vec{I}_{\mathrm{out}}$ is an $N \times 1$ vector; l is the number of spectral channels; $\boldsymbol{M}_0 = [\boldsymbol{m}_{00}, \boldsymbol{m}_{01}, \boldsymbol{m}_{02}, \boldsymbol{m}_{03}]$ is the first row of $\boldsymbol{M}(\lambda)$ (Supplementary Section 1). By minimizing the cost function with regularization, the full Stokes polarization spectrum can be reconstructed as,

$$\vec{S} = \underset{\vec{S}}{\mathrm{argmin}}\left\{ ||\vec{I}_{\mathrm{out}} - \mathbf{M}_0 \cdot \vec{S}||_2 + \mathrm{k} \cdot ||\vec{S}||_2 \right\} \tag{3}$$

where k is the regularization coefficient. Subsequently, the ellipsometry parameters can be calculated from $\vec{S}$ as

(Supplementary Section 2),

$$\Psi = \frac{1}{2}\arccos\left(-\frac{s_1}{s_0}\right) \tag{4}$$

$$\Delta = \arctan\left(\frac{s_3}{s_2}\right) \tag{5}$$

After obtaining the ellipsometry parameters, the remaining steps for the determination of thin film properties are identical to that of a conventional ellipsometry system. We can first build a multi-beam interference model for the multilayer thin film stack under test and choose a proper material model to estimate the theoretical ellipsometry parameters (Supplementary Section 3). Thereafter, by minimizing the difference between the measurement and the theoretical estimation, one can determine the thickness d and refractive index n of the thin film.

In such a framework, the key to the accurate reconstruction of the ellipsometry parameters and thin film properties is to design a metasurface array with highly anisotropic and diverse spectral features[58,59], such that the correlation coefficient of each row of the Mueller matrix can be minimized. In this work, each element of the 20×20 metasurface array is made of 300-nm-thick silicon nanopillars on a sapphire substrate. The geometry of each element is optimized by minimizing the correlation coefficient of $\boldsymbol{M}_0$ among different elements (Supplementary Section 4). Furthermore, we analyzed the system's tolerance to fabrication errors, and confirmed that it is highly robust against fabrication errors, as long as the Mueller matrix of the fabricated metasurface array is carefully recalibrated. (Supplementary Section 5).

To experimentally demonstrate the metasurface array-based spectropolarimetric detection system, we assembled a prototype as shown in Fig. 3a. The metasurface array comprises 20×20 elements with a total size of $1.5 \times 1.5\ \mathrm{mm}^2$. The metasurface array was fabricated via the standard electron-beam lithography and reactive-ion etching process on a silicon-on-sapphire substrate (see Methods). The metasurface array was integrated onto a CMOS image sensor (Sony IMX-183) with a 5-μm-thick optically clear adhesive tape. The photograph of the metasurface array and 4 representative scanning electron microscopy images of the metasurface elements are shown in Fig. 3b, c, respectively.

To calibrate $\boldsymbol{M}_0$ of the metasurface array, we used a tunable monochromatic light source sampled at a 1-nm-interval across the spectral range from 500 nm to 700 nm (see Methods and Supplementary Figs. S14–S15). To evaluate the spectropolarimetric reconstruction performance of the system, we first reconstructed several spectra with simple narrowband features and with varying polarization states. As depicted in Fig. 3d, the reconstructed full Stokes polarization spectra agree very closely with the ground truth. The reconstruction error is quantitatively evaluated using the root mean square error (RMSE) $= \left\|\frac{\vec{S}-\vec{S'}}{4\times\nu}\right\|_2$, where $\vec{S}$ is the normalized ground truth, $\vec{S'}$ is the normalized reconstruction result, and ν is the number of sampled spectral channels. The average peak-wavelength error, linewidth error, and RMSE, of the measured spectra are 0.17 nm, 0.33 nm, and 1.87%, respectively.

To further assess the system's capability to resolve fine spectral features, we prepared a linearly-polarized incident light with a double-peak spectrum by combining a semiconductor laser emitting at a wavelength of 653.5 nm with a white-light source coupled to a monochromator. As shown in Fig. 3e, the metasurface array-based spectropolarimetric detection system can clearly distinguish double spectral peaks at 653.5 nm and 662.2 nm separated by 8.7 nm. With a smaller spectral separation, the reconstructed spectrum gradually deviates from the ground truth (Supplementary Fig. S16). The relatively low spectral resolution of the system, which is lower than the theoretical resolution (Supplementary Section 6), may be due to the inaccurate calibration of the Mueller matrix and the deterioration in the anisotropic spectral response of the experimentally realized metasurface array. This issue may be addressed via inverse design[60–62] of freeform metasurface unit cells with further decreased correlation and by more accurate calibration of the Mueller matrix. Despite the moderate spectral resolution of our system, it is worth noticing that the complexity of the full Stokes polarization spectrum of a thin film is a function of the film thickness and refractive index. For most thin films with a moderate thickness (<1000 nm) and refractive index (<3), the ellipsometry parameters can still be reconstructed with high fidelity.

Finally, to experimentally demonstrate spectroscopic ellipsometry measurement, five SiO_2 thin films with thicknesses ranging from 100 nm to 1000 nm deposited on a silicon substrate were selected as samples for testing, similar to the protocol in ref. [8]. White light emitted from a halogen lamp, after passing through a 45° linear polarizer, impinged on the thin film samples at a 60° incident angle, close to the Brewster angle, to ensure significant polarization conversion. The reflected light from the thin film impinged on the metasurface array at normal incidence (Supplementary Fig. S17). The reconstructed full Stokes polarization spectra of two representative SiO_2 thin films with thicknesses of 100 nm and 1000 nm are shown in Fig. 4a, b, respectively, which are compared to the ground truth measured with a quarter-waveplate, a rotating polarizer, and a conventional grating-based spectrometer, showing excellent agreement. Reconstructed spectra for

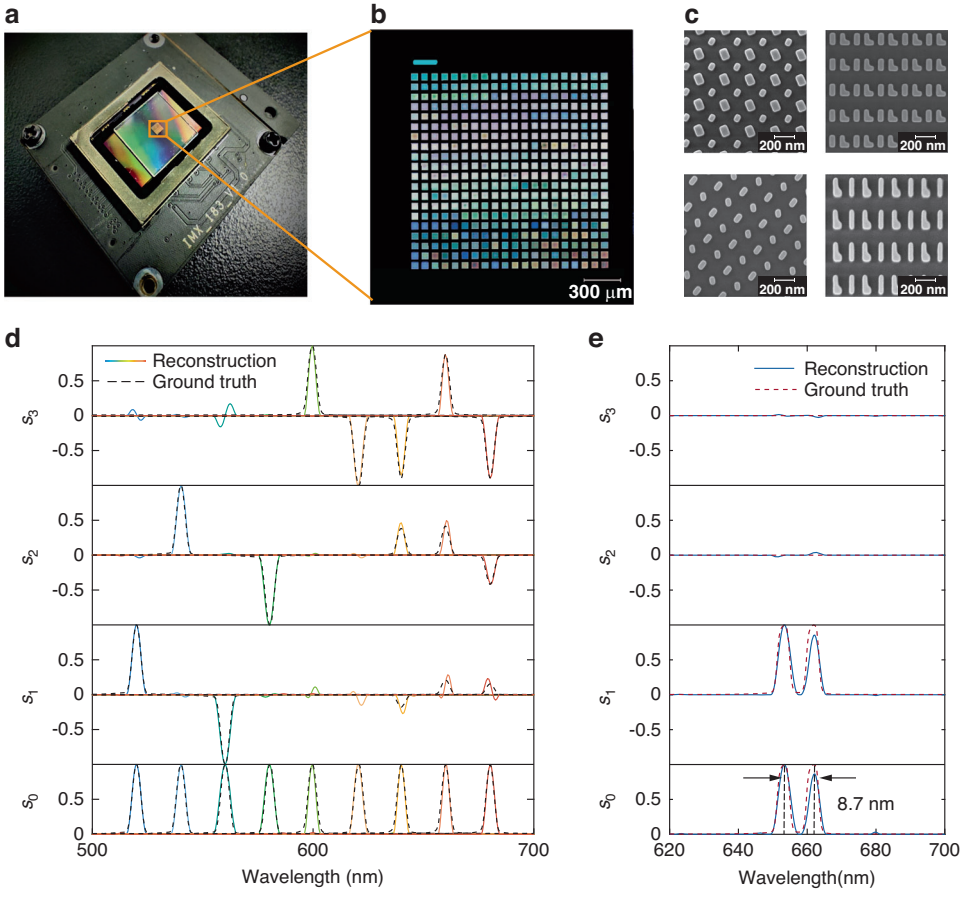

Fig. 3 Characterization of the spectropolarimetric detection performance. a Photograph of the metasurface array-based spectroscopic ellipsometer. Zoom-in photograph (**b**) and SEM images (**c**) of the fabricated metasurface array. **d** Full Stokes polarization spectra of narrowband light sources (with wavelength ranging from 520 nm to 680 nm in a 20-nm-interval, and with random polarization) measured with the metasurface array-based spectropolarimetric detection system (solid lines) compare with the ground truth measured with a quarter-waveplate, a rotating polarizer, and a conventional grating-based spectrometer (black dashed lines). **e** Reconstructed full Stokes polarization spectrum of linearly polarized light with dual spectral peaks separated by 8.7 nm measured with the metasurface array-based spectropolarimetric detection system (blue solid line) compare with the ground truth measured with a quarter-waveplate, a rotating polarizer, and a conventional grating-based spectrometer (red dashed line). The peak wavelengths are highlighted by the black dashed line. SEM scanning electron microscopy

thin films with other thicknesses can be found in Supplementary Fig. S18. A decent average RMSE of 4.5% was obtained for the five measured SiO_2 thin films.

Subsequently, the full Stokes polarization spectra can be converted to the ellipsometry parameters Ψ and Δ. The converted ellipsometry parameters of the SiO_2 thin film with thicknesses of 100 nm and 1000 nm are shown in Fig. 4c, d, respectively, which are compared with the ground truth and the theoretical estimation calculated from a three-layer model consisting of air, SiO_2, and a silicon substrate. Reconstructed ellipsometry parameters for films with other thicknesses can be found in Supplementary Fig. S18. By minimizing the squares error of the reconstruction and the theoretical estimation of Δ, the thickness and refractive index of the SiO_2 thin films can be determined. The comparison between the film thickness reconstructed from our system and the measurement from a commercial spectroscopic ellipsometer (JA Woollam, V-VASE) is shown in Fig. 4e. Using the measured thickness from the commercial spectroscopic ellipsometer as the ground truth, the accuracy of the thickness measurement, defined as the relative error between the reconstructed film thickness and the ground truth, is only 2.16% on average for the five SiO_2 thin films. The precision of the thickness measurement, defined as the standard deviation in the 10 measurements within a 10-minute timeframe, is only 1.28 nm on average for the five SiO_2 thin films (Supplementary Fig. S19). In the fitting process, the refractive index of the SiO_2 thin films was assumed to follow the Cauchy model as $n = A + \frac{B\lambda^2}{\lambda^2 - C^2} - D\lambda^2$, where A, B, C and D are the fitting parameters[63]. The

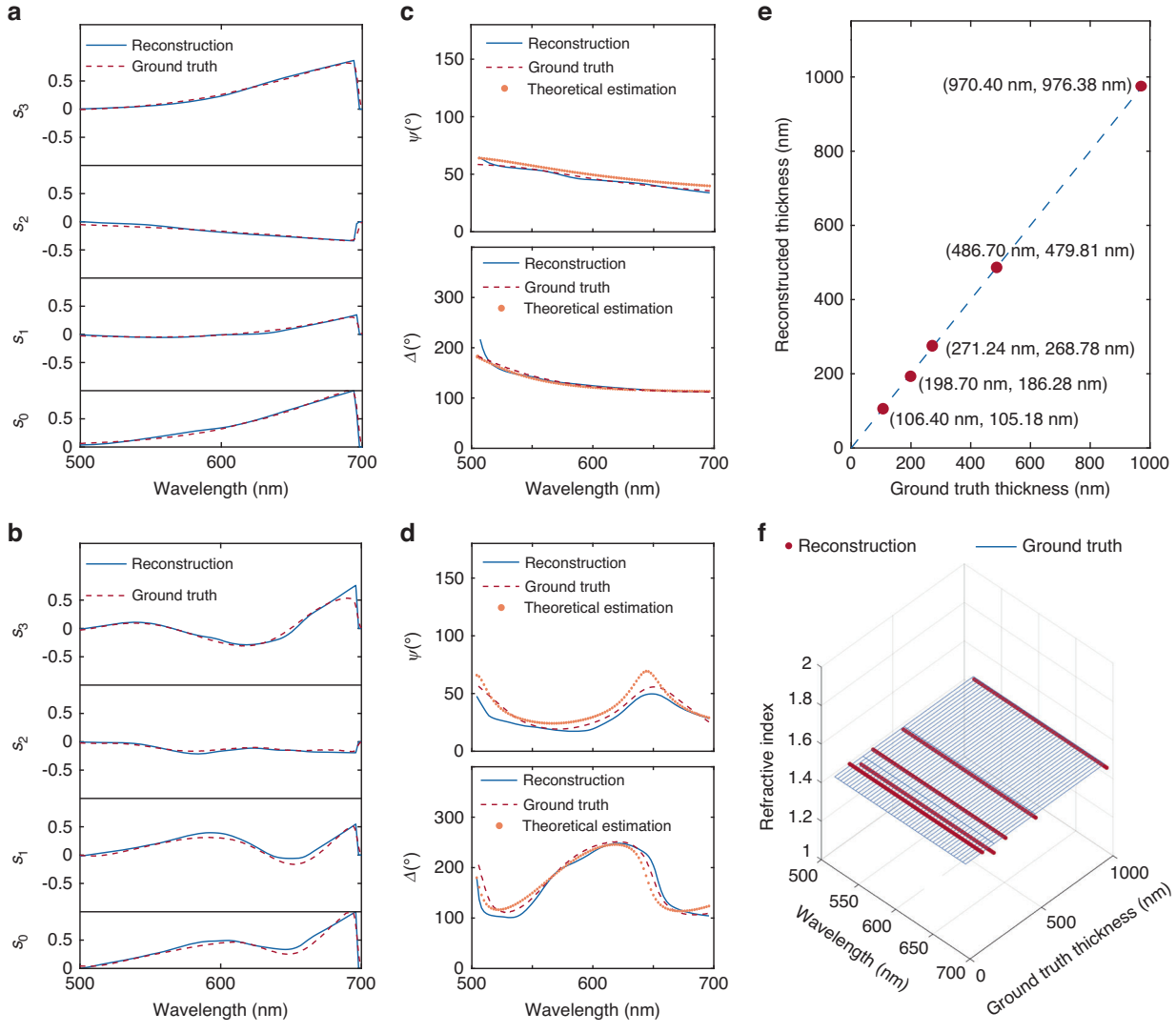

Fig. 4 Measurement of the thickness and refractive index of SiO_2 thin films. Comparison between the reconstructed full Stokes polarization spectra from the single-shot spectroscopic ellipsometer (blue solid line) and the ground truth (red dashed line) for SiO_2 thin film with a thickness of 100 nm (**a**) and 1000 nm (**b**), respectively. The ground truth is measured with a quarter-waveplate, a rotating polarizer, and a conventional grating-based spectrometer. Comparison among the ellipsometry parameters Ψ and Δ from the single-shot spectroscopic ellipsometer (blue solid line), the ground truth (red dashed line), and the theoretical estimation (orange dots) for SiO_2 thin film with a thickness of 100 nm (**c**) and 1000 nm (**d**), respectively. The ground truth is measured with a quarter-waveplate, a rotating polarizer, and a conventional grating-based spectrometer. **e** Comparison of the reconstructed thickness from the single-shot spectroscopic ellipsometer with the ground truth thickness from the commercial spectroscopic ellipsometer for five SiO_2 thin films under testing. **f** Comparison of the reconstructed refractive index (red dots) from the single-shot spectroscopic ellipsometer with the ground truth (blue grids) from fused silica refractive index data in commercial spectroscopic ellipsometer for five SiO_2 thin films under testing

reconstructed refractive index dispersions for the five SiO_2 thin films are shown in Fig. 4f, with an average accuracy and precision of 0.84% and 0.0032, respectively (Supplementary Fig. S19). The entire computational reconstruction process was implemented in MATLAB, taking ~800 ms to reconstruct the full Stokes polarization spectrum and ~200 ms to reconstruct the thin film thickness and refractive index on a desktop computer equipped with an AMD Ryzen 7 3700x CPU and 32 GB RAM. To further enhance the speed and accuracy of the reconstruction, one may implement deep learning-based algorithms for both steps[45,48,64,65].

Discussion

In conclusion, we have proposed and experimentally demonstrated a new type of metasurface array-based spectroscopic ellipsometry system for the single-shot measurement of thin film properties. Compared to

conventional spectroscopic ellipsometers, our system has no mechanical moving parts or phase-modulating elements, Consequently, it may enable high-throughput, online measurement of thin film properties in semiconductor processing, such as in a thin film etching or deposition system. In the current prototype, we only reconstructed the thickness and refractive index of a single-layer lossless film. To allow the reconstruction of multi-layer films with losses, the design and fabrication of the metasurface array, as well as the ellipsometry fitting model, shall be further improved (Supplementary Section 7). For the prototype system, the spectral range of the ellipsometry measurement is mainly limited by the low quantum efficiency of the available CMOS image sensor above the wavelength of 700 nm and the high material loss of silicon below the wavelength of 500 nm. To further extend the range, one may select a CMOS image sensor with a higher quantum efficiency in the near-infrared range or design and fabricate metasurfaces using alternative materials with lower loss across a wider spectral range, such as SiN[46]. There is no fundamental limitation to extend its application to the UV, IR or THz range. It may also be possible to further simplify the spectroscopic ellipsometry system leveraging wavelength- and polarization-dependent speckle pattern of an inexpensive, commercial optical diffuser, despite that it would require a more careful calibration process and a broadband, spatially coherent light source for illumination. The metasurface array also holds promise for spectro-polarimetric imaging, which may further allow the non-destructive characterization of spatially-inhomogeneous thin films.

Materials and methods

Metasurface fabrication

The fabrication of the metasurface was done via a commercial service offered by Tianjin H-Chip Technology Group. The fabrication process is schematically shown in Supplementary Fig. S12. The metasurface array was first patterned on a 300-nm-thick monocrystalline silicon film on a sapphire substrate by the electron beam lithography using a negative tone resist hydrogen silsesquioxane (HSQ). The next step involved transferring the pattern onto the silicon layer using HSQ as the mask via the reactive ion etching process. Finally, the HSQ resist is removed by buffered oxide etchant.

Metasurface characterization

The experiment setup for the calibration of the metasurface array response is schematically shown in Supplementary Fig. S13. A supercontinuum laser (YSL Photonics, SC-Pro-7) was coupled to a monochromator (Zolix, Omni-λ2007i) and a collimation lens to emit collimated light with a narrowband spectrum. To eliminate spatial coherence and the resulting speckles on the imaging sensor, the light passed through a rotating diffuser before reaching the metasurface array. To ensure uniform illumination on the metasurface array, we established a Köhler illumination condition using two lenses with focal lengths of 50 mm and 35 mm, respectively, along with two apertures.

To calibrate $\boldsymbol{M}_0$ of the metasurface array, its transmittance was measured with 0° linear polarization (T_x), 45° linear polarization (T_{45}), 90° linear polarization (T_y), and left-handed circular polarization (T_{lcp}), respectively. The polarization state of the incident light was adjusted by a polarizer and a broadband quarter-waveplate. For each sampled spectral channel, the grayscale image of the metasurface array was captured by the CMOS sensor. The transmittance was subsequently calculated by dividing the light intensity underneath the metasurface array by the light intensity in a blank region after the subtraction of the background noise. $\boldsymbol{M}_0$ of the metasurface array was then calculated as,

$$\mathbf{M}_0 = \begin{bmatrix} \frac{1}{2}\left(\mathrm{T_x} + \mathrm{T_y}\right) \\ \frac{1}{2}\left(\mathrm{T_x} - \mathrm{T_y}\right) \\ \mathrm{T_{45}} - \frac{1}{2}\left(\mathrm{T_x} + \mathrm{T_y}\right) \\ \frac{1}{2}\left(\mathrm{T_x} + \mathrm{T_y}\right) - \mathrm{T_{lcp}} \end{bmatrix}^{\mathrm{T}} \tag{6}$$

Acknowledgements
This work was supported by the National Natural Science Foundation of China (62135008, 61975251) and by the Guoqiang Institute, Tsinghua University.

Author contributions
Y.Y., S.W. and X.X. conceived this work. S.W. and X.X. designed and characterized the metasurface, developed the spectropolarimetric reconstruction algorithm, built the metasurface array-based spectroscopic ellipsometer system, and measured the thin film properties; S.W., X.X., L.S., S.W., Y.N., and Y.Y. analyzed the data; S.W., X.X., and Y.Y. wrote the manuscript. Y.Y. supervised the project.

Conflict of interest
The authors declare no competing interests.

Supplementary information The online version contains supplementary material available at https://doi.org/10.1038/s41377-024-01396-3.

Received: 27 September 2023 Revised: 3 January 2024 Accepted: 24 January 2024
Published online: 10 April 2024

References

1. McCrackin, F. L. et al. Measurement of the thickness and refractive index of very thin films and the optical properties of surfaces by ellipsometry. *J. Res. Natl. Bur. Stand.- A. Phys. Chem.* **67A**, 363–377 (1963).
2. Azzam, R. M. A., Bashara, N. M. & Ballard, S. S. Ellipsometry and polarized light. *Phys. Today* **31**, 72 (1978).
3. Vedam, K. Spectroscopic ellipsometry: a historical overview. *Thin Solid Films* **313-314**, 1–9 (1998).
4. Kwak, H. et al. Non-destructive thickness characterisation of 3D multilayer semiconductor devices using optical spectral measurements and machine learning[J]. *Light: Adv. Manufact.* **2**, 1 (2021).

5. Irene, E. A. Applications of spectroscopic ellipsometry to microelectronics. *Thin Solid Films* **233**, 96–111 (1993).
6. Schubert, M. *Infrared Ellipsometry on Semiconductor Layer Structures - Phonons, Plasmons, and Polaritons*. (Berlin: Springer, 2004).
7. Fujiwara, H. & Kondo, M. Real-time monitoring and process control in amorphous/crystalline silicon heterojunction solar cells by spectroscopic ellipsometry and infrared spectroscopy. *Appl. Phys. Lett.* **86**, 032112 (2005).
8. Collins, R. W. & Koh, J. Dual rotating-compensator multichannel ellipsometer: instrument design for real-time Mueller matrix spectroscopy of surfaces and films. *J. Opt. Soc. Am. A* **16**, 1997–2006 (1999).
9. Shan, A. et al. High-speed imaging/mapping spectroscopic ellipsometry for in-line analysis of roll-to-roll thin-film photovoltaics. *IEEE J. Photovolt.* **4**, 355–361 (2014).
10. Petrik, P. & Fried, M. Mapping and imaging of thin films on large surfaces. *Phys. Status Solidi (A)* **219**, 2100800 (2022).
11. Jellison, G. E. & Modine, F. A. Two-modulator generalized ellipsometry: theory. *Appl. Opt.* **36**, 8190–8198 (1997).
12. Azzam, R. M. A. Division-of-amplitude photopolarimeter (DOAP) for the simultaneous measurement of all four stokes parameters of light. *Opt. Acta: Int. J. Opt.* **29**, 685–689 (1982).
13. Lee, J. et al. Rotating-compensator multichannel ellipsometry: applications for real time stokes vector spectroscopy of thin film growth. *Rev. Sci. Instrum.* **69**, 1800–1810 (1998).
14. Fujiwara, H. *Spectroscopic Ellipsometry: Principles and Applications*. (Hoboken: Wiley, 2007).
15. Chen, C., An, I. & Collins, R. W. Multichannel mueller matrix ellipsometry for simultaneous real-time measurement of bulk isotropic and surface anisotropic complex dielectric functions of semiconductors. *Phys. Rev. Lett.* **90**, 217402 (2003).
16. Collins, R. W. et al. *Multichannel ellipsometry. in Handbook of Ellipsometry* (eds Tompkins, H. G. & Irene, E. A.) (Norwich: William Andrew Publishing, 2005).
17. Mukherjee, D. & Petrik, P. Real-time ellipsometry at high and low temperatures. *ACS Omega* **8**, 3684–3697 (2023).
18. Minamikawa, T. et al. Dual-comb spectroscopic ellipsometry. *Nat. Commun.* **8**, 610 (2017).
19. Zhang, R. X. et al. Dynamic ellipsometry measurement based on a simplified phase-stable dual-comb system. *Optics Express* **30**, 7806–7820 (2022).
20. Yu, N. F. et al. Light propagation with phase discontinuities: generalized laws of reflection and refraction. *Science* **334**, 333–337 (2011).
21. Lin, D. M. et al. Dielectric gradient metasurface optical elements. *Science* **345**, 298–302 (2014).
22. Yu, N. F. & Capasso, F. Flat optics with designer metasurfaces. *Nat. Mater.* **13**, 139–150 (2014).
23. Yang, Y. M. et al. Dielectric meta-reflectarray for broadband linear polarization conversion and optical vortex generation. *Nano Lett.* **14**, 1394–1399 (2014).
24. Zhu, Y. et al. Metasurfaces designed by a bidirectional deep neural network and iterative algorithm for generating quantitative field distributions[J]. *Light: Adv. Manufact.* **4**, 9 (2023).
25. Lee, G. Y. et al. Complete amplitude and phase control of light using broadband holographic metasurfaces. *Nanoscale* **10**, 4237–4245 (2018).
26. Overvig, A. C. et al. Dielectric metasurfaces for complete and independent control of the optical amplitude and phase. *Light Sci. Appl.* **8**, 92 (2019).
27. Kwon, H. et al. Single-shot quantitative phase gradient microscopy using a system of multifunctional metasurfaces. *Nat. Photonics* **14**, 109–114 (2020).
28. Wen, L. et al. Broad-band spatial light modulation with dual epsilon-near-zero modes. *Opto-Electron. Adv.* **5**, 200093 (2022).
29. Wei, J. X. et al. Mid-infrared semimetal polarization detectors with configurable polarity transition. *Nat. Photonics* **15**, 614–621 (2021).
30. Dorrah, A. H. et al. Structuring total angular momentum of light along the propagation direction with polarization-controlled meta-optics. *Nat. Commun.* **12**, 6249 (2021).
31. Shen, Z. C. et al. Monocular metasurface camera for passive single-shot 4D imaging. *Nat. Commun.* **14**, 1035 (2023).
32. Sautter, J. et al. Active tuning of all-dielectric metasurfaces. *ACS Nano* **9**, 4308–4315 (2015).
33. Devlin, R. C. et al. Broadband high-efficiency dielectric metasurfaces for the visible spectrum. *Proc. Natl. Acad. Sci. USA* **113**, 10473–10478 (2016).
34. Zhao, F. et al. Metalens-assisted system for underwater imaging. *Laser Photonics Rev.* **15**, 2100097 (2021).
35. Ren, Y. Z. et al. Full-stokes polarimetry for visible light enabled by an all-dielectric metasurface. *Adv. Photonics Res.* **3**, 2100373 (2022).
36. Arbabi, E. et al. Full-stokes imaging polarimetry using dielectric metasurfaces. *ACS Photonics* **5**, 3132–3140 (2018).
37. Yang, Z. Y. et al. Generalized Hartmann-Shack array of dielectric metalens sub-arrays for polarimetric beam profiling. *Nat. Commun.* **9**, 4607 (2018).
38. Rubin, N. A. et al. Matrix Fourier optics enables a compact full-Stokes polarization camera. *Science* **365**, eaax1839 (2019).
39. Shaltout, A. et al. Photonic spin Hall effect in gap-plasmon metasurfaces for on-chip chiroptical spectroscopy. *Optica* **2**, 860–863 (2015).
40. Pors, A., Nielsen, M. G. & Bozhevolnyi, S. I. Plasmonic metagratings for simultaneous determination of Stokes parameters. *Optica* **2**, 716–723 (2015).
41. Tittl, A. et al. Imaging-based molecular barcoding with pixelated dielectric metasurfaces. *Science* **360**, 1105–1109 (2018).
42. Yesilkoy, F. et al. Ultrasensitive hyperspectral imaging and biodetection enabled by dielectric metasurfaces. *Nat. Photonics* **13**, 390–396 (2019).
43. Wang, Z. et al. Single-shot on-chip spectral sensors based on photonic crystal slabs. *Nat. Commun.* **10**, 1020 (2019).
44. Yoon, H. H. et al. Miniaturized spectrometers with a tunable van der Waals junction. *Science* **378**, 296–299 (2022).
45. Yang, Z. Y. et al. Miniaturization of optical spectrometers. *Science* **371**, eabe0722 (2021).
46. Zhu, Y. B. et al. Compact CMOS spectral sensor for the visible spectrum.*Photonics Res.* **7**, 961–966 (2019).
47. Cen, Q. et al. Microtaper leaky-mode spectrometer with picometer resolution. *eLight* **3**, 9 (2023).
48. Zhang, W. Y. et al. Deeply learned broadband encoding stochastic hyperspectral imaging. *Light Sci. Appl.* **10**, 108 (2021).
49. Xiong, J. et al. Dynamic brain spectrum acquired by a real-time ultraspectral imaging chip with reconfigurable metasurfaces. *Optica* **9**, 461–468 (2022).
50. Yang, J. W. et al. Ultraspectral imaging based on metasurfaces with freeform shaped meta-atoms. *Laser Photonics Rev.* **16**, 2100663 (2022).
51. Yako, M. et al. Video-rate hyperspectral camera based on a CMOS-compatible random array of Fabry-Pérot filters. *Nat. Photonics* **17**, 218–223 (2023).
52. Chen, W. T. et al. Integrated plasmonic metasurfaces for spectropolarimetry. *Nanotechnology* **27**, 224002 (2016).
53. Maguid, E. et al. Photonic spin-controlled multifunctional shared-aperture antenna array. *Science* **352**, 1202–1206 (2016).
54. Ding, F. et al. Beam-size-invariant spectropolarimeters using gap-plasmon metasurfaces. *ACS Photonics* **4**, 943–949 (2017).
55. Chen, Y. T. et al. On-chip spectropolarimetry by fingerprinting with random surface arrays of nanoparticles. *ACS Photonics* **5**, 1703–1710 (2018).
56. Shinoda, K. & Ohtera, Y. Alignment-free filter array: snapshot multispectral polarization imaging based on a Voronoi-like random photonic crystal filter. *Opt. Express* **28**, 38867–38882 (2020).
57. Ni, Y. B. et al. Computational spectropolarimetry with a tunable liquid crystal metasurface. *eLight* **2**, 23 (2022).
58. Wu, C. et al. Spectrally selective chiral silicon metasurfaces based on infrared Fano resonances. *Nat. Commun.* **5**, 3892 (2014).
59. Wang, S. et al. Arbitrary polarization conversion dichroism metasurfaces for all-in-one full Poincaré sphere polarizers. *Light Sci. Appl.* **10**, 24 (2021).
60. Molesky, S. et al. Inverse design in nanophotonics. *Nat. Photonics* **12**, 659–670 (2018).
61. Piggott, A. Y. et al. Inverse design and demonstration of a compact and broadband on-chip wavelength demultiplexer. *Nat. Photonics* **9**, 374–377 (2015).
62. Wang, S. et al. Metasurface-based solid poincaré sphere polarizer. *Phys. Rev. Lett.* **130**, 123801 (2023).
63. Herzinger, C. M. et al. Ellipsometric determination of optical constants for silicon and thermally grown silicon dioxide via a multi-sample, multi-wavelength, multi-angle investigation. *J. Appl. Phys.* **83**, 3323–3336 (1998).
64. Tua, D. et al. Imaging-based intelligent spectrometer on a plasmonic rainbow chip. *Nat. Commun.* **14**, 1902 (2023).
65. Liu, J. C. et al. Machine learning powered ellipsometry. *Light Sci. Appl.* **10**, 55 (2021).